A compact flat solar still with high performance

Guilong Peng [a], Swellam W. Sharshir [a,b,c], Zhixiang Hu [b], Rencai Ji [a], Jianqiang Ma [a], A.E. Kabeel [d,e], Huan Liu [b], Jianfeng Zang [b], Nuo Yang [a,*]

[a] State Key Laboratory of Coal Combustion, and School of Energy, and Power Engineering, Huazhong University of Science and Technology, Wuhan 430074, China
[b] School of Optical and Electronic Information, Huazhong University of Science and Technology, Wuhan 430074, China
[c] Mechanical Engineering Department, Faculty of Engineering, Kafrelsheikh University, Kafrelsheikh, Egypt
[d] Mechanical Power Engineering Department, Faculty of Engineering, Tanta University, Tanta, Egypt
[e] Faculty of Engineering, Delta University for Science and Technology, Gamasa, Egypt

ARTICLE INFO

ABSTRACT

Solar still is a convenient off-grid device for desalination, which can provide fresh water for families, ships, islands, and so on. The conventional inclined solar still (ISS) suffers from low efficiency and low productivity. To improve the performance of solar still, a flat solar still (FSS) is proposed, which has a working principle similar to the solar cell. The condensate water in FSS is collected by the capillary grid attached under the ultra-hydrophilic glass cover, instead of by gravity. Therefore, FSS avoids the inclined structure and is much more compact than ISS. The daily productivity of FSS reaches up to 4.3 kg/m^2 under 6.3 kWh/m^2 of solar insolation. Theoretical analysis shows that the enhanced mass transfer in FSS by the compact structure is an important factor for high performance. More interestingly, FSS can also be easily extended to more stages for latent heat recovery. The results show that the daily productivity and energy efficiency of a double-stage FSS reaches up to 7 kg/m^2 and 72%, respectively, under 6.7 kWh/m^2 of solar insolation, which is much higher than the conventional solar still. FSS paves a new way in designing and optimizing solar still.

1. Introduction

Freshwater is of major importance to human beings' survival as well as our economic activities such as agriculture and industry. Nowadays billions of people are suffering from freshwater scarcity [1]. Thereby, it is highly desirable to find out effective ways to get fresh water from alternative resources such as wastewater, brackish, ground, seawater, and so on [2]. Desalination is a promising technology to meet the global freshwater demand, due to saline water account for 97% of the water on the earth's surface. Furthermore, solar desalination is considered as one type of desalination technology, which has many benefits such as no fuel cost and eco-friendly [3,4].

The solar still, a typical small-scale solar desalination system, provides a solution for the water shortage problem in remote regions, arid areas, and emergencies, etc. [5]. Solar still has many special features such as low fabrication cost, easy to maintain, and portable [6]. The great majority of the investigated solar stills are inclined solar still (ISS), which mainly consists of a wedge-shaped basin and glass cover [7–9]. However, solar still is not universally utilized due to the relatively low productivity as well as the low energy efficiency [10–12].

To improve the productivity as well as the thermal performance of the solar still, many studies have been carried out by different methods, such as improving the structure by designing stepped solar still [13–15], wick type solar still [16–18], double slope solar still [19,20], pyramid solar still [21] and so on. Using special materials is another effective way, such as porous materials for enhancing the temperature difference between water and the condensing cover as well as evaporation area [22,23], graphite or charcoal for enhancing solar absorption and heat transfer [24,25], phase change materials for heat storage [26–28] and so forth. Nowadays, the productivity of ISS is usually 2-5 kg/m^2 per day and the corresponding energy efficiency is around 30-50% [7,29–32]. Therefore, there is still ample room for further improvements.

In recent years, many efforts have been done to improve the performance of solar still by using micro/nanostructured porous materials [33,34], such as plasmonic metals [35], carbon-based materials [36], polymers [37], and semiconductors [38]. Many new materials could exhibit high solar absorptivity (>98%) across the solar spectrum [39], which indicates few energy losses during

Nomenclature

CB	Carbon black
Cp_v	Specific heat capacity of the vapor [J/(kg·K)]
D	Diffusion coefficient of water vapor [m²/s]
Gr	Grashof number
FSS	Flat solar still
g	Gravitational acceleration [m/s²]
H	Height of the vapor chamber [m]
h_a	Convective heat transfer coefficient on the glass cover [W/(m²·K)]
h_h	Convective heat transfer coefficient in solar still [W/(m²·K)]
h_m	Convective mass transfer coefficient [m/s]
h_{fg}	Latent heat of vapor [J/kg]
h_{LV}	Total enthalpy of phase change [J/kg]
I	Solar intensity [W/m²]
ISS	Inclined solar still
L_t	Length of vertical thread [cm]
$\dot{m}$	Productivity of the solar still [kg/(m²·s)]
Nu	Nusselt number
Pr	Prandtl number
P_s	Saturated vapor pressure [Pa]
$q_{c(g\_a)}$	Heat convection between the glass cover and the ambient [J/m²]
$q_{c(w\_g)}$	Heat convection between the wick material and the glass cover [J/m²]
$q_{d(w\_b)}$	Heat conduction between the wick material and the basin [J/m²]
$q_{e(w\_g)}$	Heat of phase change [J/m²]
$q_{r(g\_a)}$	Heat radiation between the glass cover and the ambient [J/m²]
$q_{r(w\_g)}$	Heat radiation between the wick material and the glass cover [J/m²]
$R_{g,v}$	Gas constant of vapor [J/(kg·K)]
S_η	Uncertainty of energy efficiency
SG	Soda-lime glass
T_{amb}	Ambient temperature [K]
T_g	Temperature of the glass cover [K]
T_s	Temperature of the saturated moist air [K]
T_{sky}	Temperature of the sky [K]
T_w	Temperature of the wetted black wick material [K]
$T_{w,b}$	Temperature of the bulk water [K]
UG	Ultra-hydrophilic glass

Greek letters

α	Thermal diffusivity of moist air [m²/s]
α_v	Volume expansion coefficient of moist air [1/K]
β	Transmittance of the glass cover
δ_i	Thickness of the foam [m]
ε_1	Emissivity between the wick material and the glass cover
ε_2	Emissivity between the glass cover and the ambient
ε_w	Emissivity of the wick material
ε_g	Emissivity of the glass cover
ε_a	Emissivity of the ambient
η	Energy efficiency of solar still
λ_i	Thermal conductivity of the foam [W/(m·K)]
ν	Kinematic viscosity [m²/s]
ρ_v	Density of the vapor [kg/m³]
σ	Stefan-Boltzmann constant [W/(m²·K⁴)]
τ	Solar absorptivity of the wick material

the solar absorption process. With high solar absorptivity and ad-

vanced interfacial evaporation strategy, the energy efficiency of the evaporation process can reach up to more than 90% [4,40]. Therefore, the state-of-the-art technologies almost push the efficiency of the solar absorption process and evaporation process to the limitation.

Nevertheless, simply applying micro/nano-materials to conventional solar stills might obtain poor productivity. Many works reported that solar stills with advanced micro/nano-materials are about 1-4 kg/day and the corresponding efficiency is below 40% under the natural sun, which is similar to the solar still without micro/nano-materials [41–44]. It is found that the inefficient results from the inherent disadvantages of conventional ISS, such as the inefficient condensation, solar reflection by condensate droplets, the large heat loss of the system, and so on [34,42]. Therefore, there is a demand for designing new types of solar stills for solving these problems and effectively improving the system performance.

Therefore, some new kinds of solar stills are studied recently, such as the thermal concentrated or thermally-localized solar still [45,46]. In the state-of-the-art thermally-localized solar still, the evaporated water is replenished by thin hydrophilic membranes at each stage. The productivity of a 10-stage solar still can reach up to more than 2 L/(kW•h) under natural solar irradiation [47,48]. Nevertheless, the application of such kinds of solar stills for continuously working and large-scale utilization remains a challenge, due to the salt crystallization on hydrophilic membranes or a large number of metallic fins required for cooling.

In this paper, by imitating the working principle of the solar cell, a high-performance flat solar still (FSS) is proposed, which breaks the stereotype and makes innovation in solar still. Similar to that electrons are collected by the metallic grid in solar cell, water molecules are produced by solar energy and collected by the capillary grid in the flat solar still. FSS is capable of working continuously with neither salt crystallization on the evaporation surface nor the necessity of massive metallic fins for cooling. To illustrate the advantages of FSS, firstly, indoor experiments by using solar simulators are carried out to explore the effect of different factors on FSS. Theoretical analysis is also carried out to uncover the advantages of FSS. Then, the potential of constructing high-efficiency double-stage FSS is verified and discussed. The proposed FSS shows great potential for large-scale application and may open a new avenue for a solar still system.

2. Materials and methods

2.1. Experimental setup and materials

To show the difference between ISS and FSS, the schematic diagram of ISS and FSS are illustrated in Fig. 1a and b. In conventional ISS, the basin is wedge-shaped where brackish/saline water is collected at its base. The wall of the basin in ISS is relatively high to ensure the inclined structure for water collecting. When the system works during the daytime, solar irradiation entering the still through the glass and is absorbed by solar absorbing materials or water. The water is heated up by solar irradiation and evaporates. The upper surface of the basin is covered by a sealed glass cover, the hot vapor flows up and condenses on the glass cover. The condensate water slides down due to gravity and accumulates outside the still as freshwater.

In FSS, the inclined structure is avoided, the condensate water on the glass cover is collected by the capillary action of cotton threads. Thereby, the four walls of the basin in FSS have the same height and can be much lower than that in ISS (Fig. 1b) hence the areas of walls are significantly decreased and the structure is much more compact. The compact structure enhances the mass transfer between the evaporation surface and the glass cover, which will
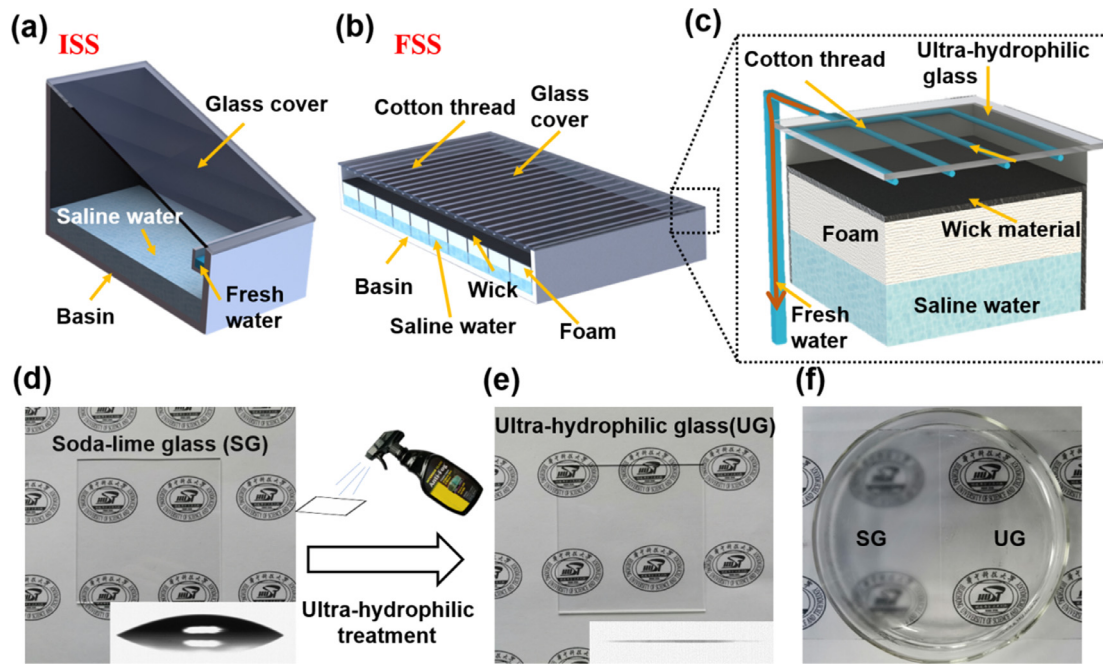
Fig. 1. Setup and materials of inclined solar still (ISS) and flat solar still (FSS). The schematic diagram of (a) a conventional ISS and (b) the proposed FSS. (c) Configuration details of FSS. The picture of (d) conventional soda-lime glass (SG) and (e) the ultra-hydrophilic glass (UG), the insert shows the contact angle of the glass. (f) SG and UG above hot water. Condensate water on UG forms a continuous film and is more transparent than SG.
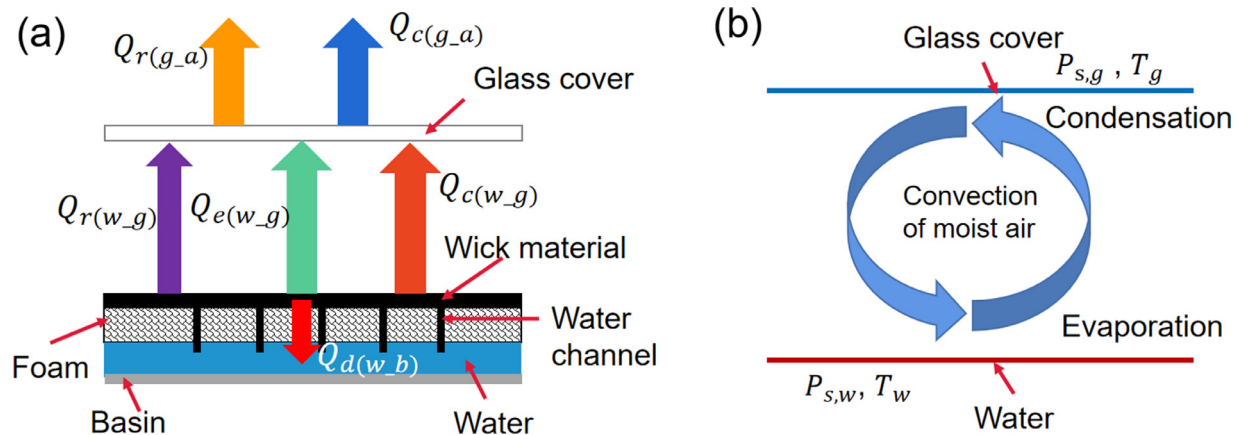
Fig. 2. (a) The schematic diagram of heat transfer in solar still. (b) The schematic diagram of the mass transfer process by the natural convection of air.

be discussed later. Meanwhile, latent heat recovery is of significant importance for enhancing the daily productivity of solar still [34]. FSS can be easily extended to more stages for latent heat recovery, due to the flat and compact structure. On the contrary, most of the conventional ISS has either complex system configuration or unsatisfying performance for latent heat recovery [49–51]. Therefore, compared with the ISS system, FSS has two very important advantages due to the improved system design: enhanced mass transfer rate and latent heat recovery performance.

The detailed schematic diagram of FSS is shown in Fig. 1c. The basin of FSS is made of foam and galvanized iron sheet, which contains saline water and prevents heat loss. Several foam strips float on the saline water and support the wick material on it (Figure S3). The foam used in this work is water-proof, which has low thermal conductivity and prevents the heat transfer between the black wick material and the bulk water. Saline water is transported from the basin to the black wick material (linen in this work) by capillary action, then heated by solar energy and evaporates. The

floating foam and wick material enable heat localization and high-efficiency evaporation at the air-water interface [52,53].

Meanwhile, carbon black (CB) nanoparticles are dispersed on the surface of wick material to enhance solar absorption and vapor generation. The top basin is sealed by a glass cover and several cotton threads are attached to the glass cover parallelly and uniformly. To fix the cotton threads, one end of the thread is tied on the wall through a small hole, the other end connects with a weight to make the thread tighten and attaches the glass cover. The schematic diagram of how to fix the threads is shown in Fig. S5(c). When condensate water accumulates on the glass cover, it will be absorbed by the cotton threads. Later, the water absorbed by the threads will be transported out of FSS through capillary force and drop down as freshwater. More details of the materials and setup can be found in Supplementary Information, Section I-III.

To make FSS more efficient, the glass cover is treated to be ultra-hydrophilic. In this work, the conventional glass cover is
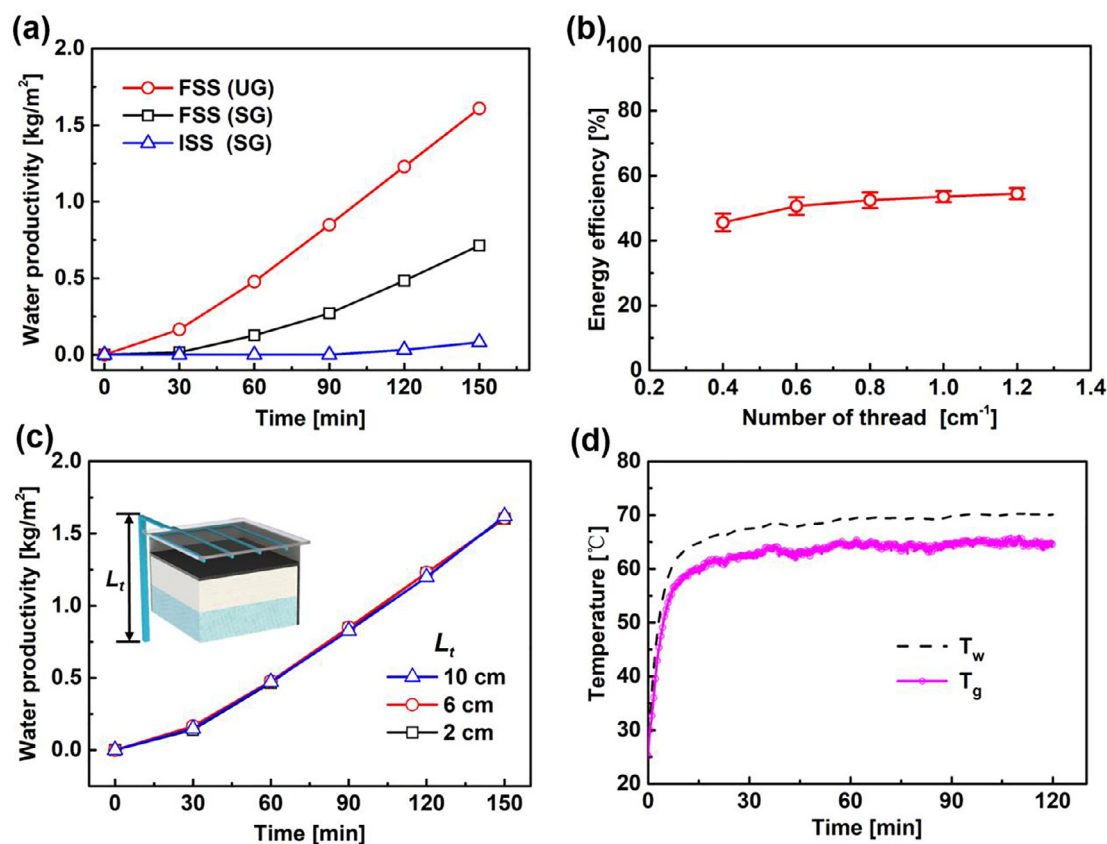
Fig. 3. Performance of a small flat solar still (FSS) and inclined solar still (ISS) in the laboratory. (a) Water productivity of FSS with ultra-hydrophilic glass (UG) and conventional soda-lime glass (SG), as well as water productivity of a conventional ISS with soda-lime glass (SG). (b) The energy efficiency of FSS with the different number of cotton threads attached to UG. (c) The productivity of FSS with different lengths of vertical cotton thread, L_t. (d) Temperatures of glass cover (T_g) and water at evaporation surface (T_w) in FSS. The number of cotton threads and length of vertical threads is 1 cm^{-1} and 6 cm, respectively. The distance between the evaporation surface and glass cover is 5 mm.

soda-lime glass (SG) which has high transparency as shown in Fig. 1d. The ultra-hydrophilic glass cover is fabricated by applying an anti-fog coating on the soda glass cover in the laboratory. The soda glass cover is fabricated by Luoyang Glass Co., Ltd., and the Rain-X anti-fog coating is fabricated by Illinois tools works Inc. The contact angle before and after treatment is shown in the insert figure of Fig. 1d and e, which shows that the contact angle decreases significantly after treatment. The method used in this work for ultra-hydrophilic treatment is only an example. Other materials or methods might also be applied, such as using commercial anti-fog film, coating SiO_2 nanoparticles [54], TiO_2 nanoparticles [55], and TiO_2 nanofibers [56] et al.

The low contact angle of glass allows vapor to condense into a continuous thin film, which has two benefits. Firstly, the glass will remain clear during the condensation process, hence more solar irradiation will enter the solar still. As shown in Fig. 1f, the patterns under SG are vague due to the light diffusion and reflection by the small condensate droplets. On the contrary, the patterns under ultra-hydrophilic glass (UG) are clear and bright. Secondly, the continuous water film accelerates water transportation from glass to threads. The water film combines all the condensate water as a whole and connects with the cotton threads. Therefore, the condensate water can be absorbed by cotton threads immediately, instead of hanging under the glass as discrete droplets as happened in SG.

2.2. Uncertainty analysis

In the indoor experiment, a solar simulator (CEL-S500 + AM1.5 filter) was used to generate the solar beam, the solar intensity

Table 1
Specification of main devices in laboratory experiments.

Name	Type	Range	Error
Electronic balance	QUINTIX224-1CN	0–220 g	±0.001g
Power meter	PM150-50C	300 mW-150 W	±2%
Thermal couple	TT-T-40-SLE	-200-260°C	±0.5°C
Data collector	Keithley 2700	1-80 Channel	$6^{1/2}$
Solar simulator	CEL-S500	800-3000 W/m^2	±1%

was measured by a power meter (PM-150-50C). The mass of collected water was measured by an electric balance (Sartorius Practum 224). The temperature was measured by T type thermal couple (Omega, TT-T-40-SLE), and a data acquisition device (Keithley 2700) was used to record the temperature. In the outdoor experiment, the solar intensity was measured and recorded every 5 seconds by a pyranometer (TBQ-2) and a voltmeter (Keysight 34401A). The temperatures of the ambient and solar stills are measured by thermal couples (Omega TT-K-36-SLE) and a thermometer (TES-1310). The mass of the collected water was measured by a portable electric balance (K-FINE 500). More details can be found in Supporting Information I-II. The Errors of devices are shown in Tables 1 and 2.

Propagation of uncertainty is the uncertainty of estimated value obtained from the uncertainty of measured parameters. The errors in the productivity of the indoor and outdoor experiment are mainly attributed to the error of electronic balance, which can be ignored due to the error is less than 1%. On the other hand, the error in the energy efficiency of solar stills is mainly caused by the power meter and solar simulator. The uncertainty of energy effi-
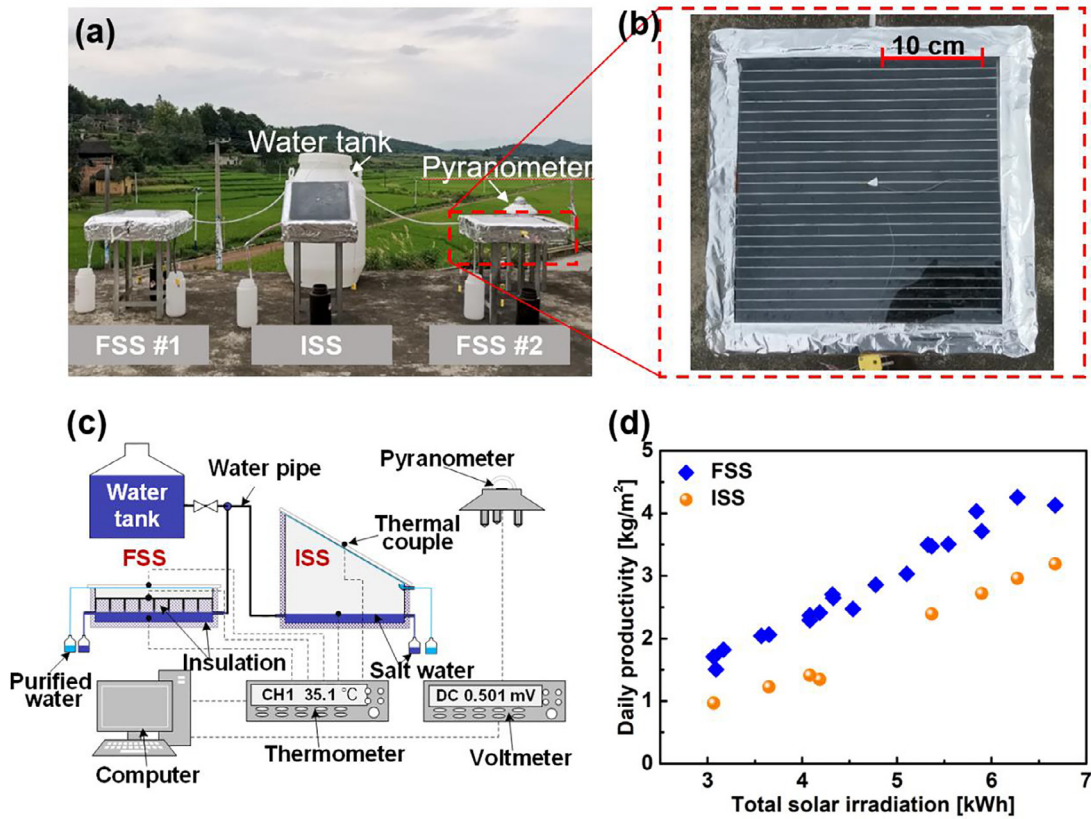
Fig. 4. Outdoor experiment setup and results. (a) The photo of ISS and FSS during outdoor experiments. (b) Top view of the FSS with the size 25 cm × 25 cm. (c) The schematic diagram of measurement setup in outdoor experiments. (d) The productivity of FSS and ISS under different daily solar irradiation.

Table 2
Specification of main devices in outdoor experiments.

Name	Type	Range	Error
Electronic balance	K-FINE 500	0-500 g	±0.05g
Pyranometer	TBQ-2	0 -2000 W/m²	±8%
Thermal couple	Omega TT-K-36-SLE	-267-260°C	±0.5°C
Thermometer	TES-1310	-50-1300°C	±0.1°C
Voltmeter	Keysight 34401A	0-1000 V	±0.005%

ciency is:

$$S_\eta = \sqrt{\left(\frac{\partial \eta}{\partial \dot{m}}\right)^2 S_{\dot{m}}{}^2 + \left(\frac{\partial \eta}{\partial I}\right)^2 S_I{}^2} \tag{1}$$

$$\eta = \frac{\dot{m} \cdot h_{LV}}{\int I dt} \times 100\% \tag{2}$$

where η is energy efficiency, $\dot{m}$ is the productivity, I is the solar intensity. h_{LV} is the total enthalpy of phase change. The daily accumulative measurement error of outdoor solar energy by pyranometer is 8%.

2.3. Theoretical model

The schematic diagram of the heat and mass transfer process in solar still is shown in Fig. 2. Based on the energy conservation, it can be obtained that,

$$\tau \beta I = q_{r(w\_g)} + q_{d(w\_b)} + q_{e(w\_g)} + q_{c(w\_g)} \tag{3}$$

$$q_{r(w\_g)} + q_{e(w\_g)} + q_{c(w\_g)} = q_{r(g\_a)} + q_{c(g\_a)} \tag{4}$$

where τ is the solar absorptivity of the carbon black coated wick material, β is the transmittance of the glass cover. $q_{r(w\_g)}$, $q_{e(w\_g)}$, $q_{c(w\_g)}$ are the heat transferred from the wick material to the glass cover by radiation, phase change, and convection, respectively. $q_{d(w\_b)}$ is the heat conducted from the wick material to the basin. $q_{r(g\_a)}$, $q_{c(g\_a)}$ are the heat transferred from the glass to the ambient by radiation and convection, respectively.

The heat transferred by irradiation are:

$$q_{r(w\_g)} = \varepsilon_1 \sigma \left(T_w{}^4 - T_g{}^4\right) \tag{5}$$

$$q_{r(g\_a)} = \varepsilon_2 \sigma \left(T_g{}^4 - T_{sky}{}^4\right) \tag{6}$$

where $\sigma = 5.67 \times 10^{-8} \, W/(m^2 \cdot K^4)$ is the Stefan-Boltzmann constant, T_w, T_g, T_{sky} are the temperature of wick material, glass cover, and sky, respectively. ε is the emissivity and is obtained by [57]:

$$\varepsilon_1 = \left[\frac{1}{\varepsilon_w} + \frac{1}{\varepsilon_g} - 1\right]^{-1} \tag{7}$$

$$\varepsilon_2 = \left[\frac{1}{\varepsilon_a} + \frac{1}{\varepsilon_g} - 1\right]^{-1} \tag{8}$$

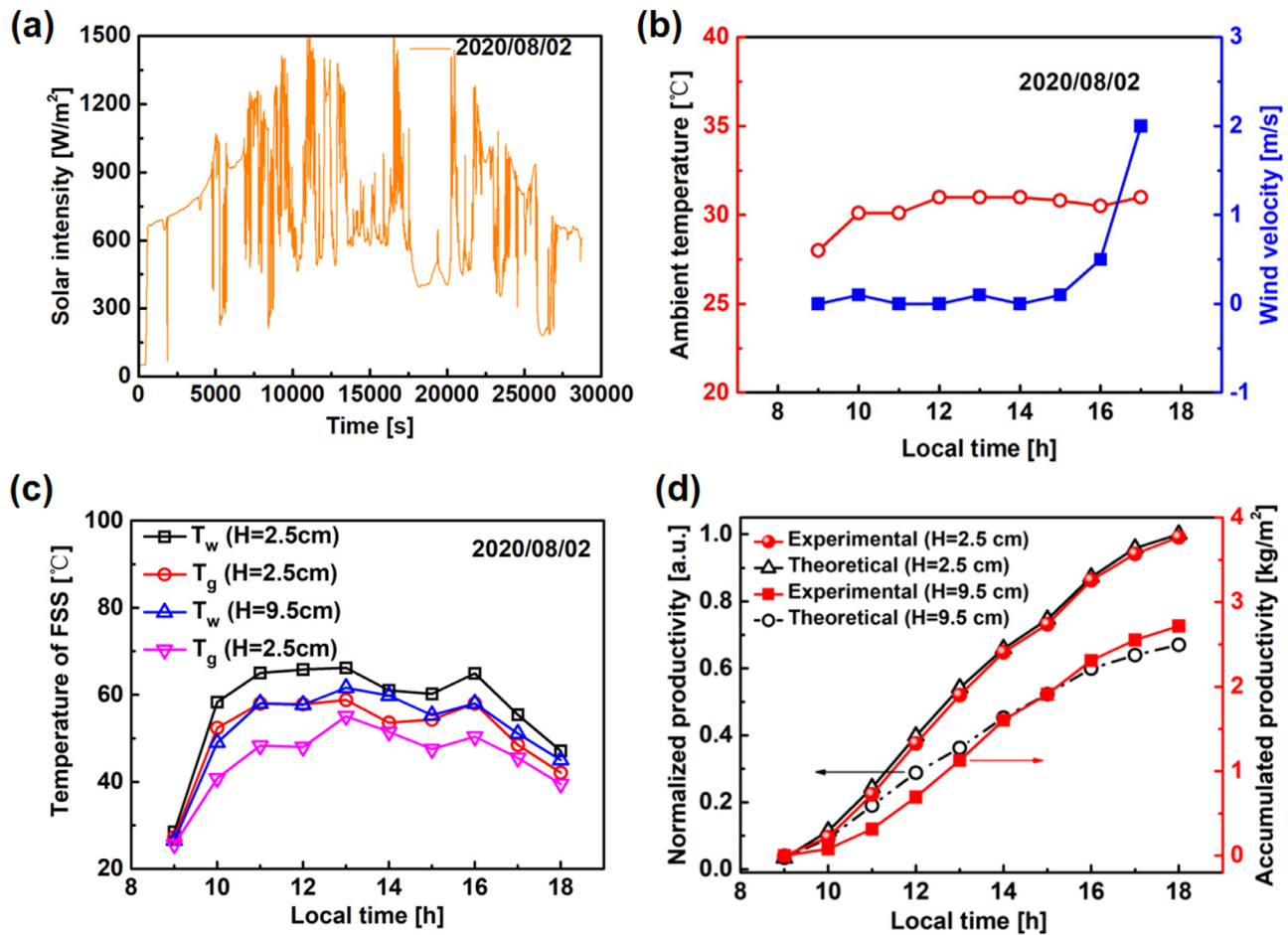Herein, ε_w, ε_g and ε_a are 0.95, 0.94 and 1, respectivily. T_{sky} is related to the ambient temperature T_{amb} [19]:

$$T_{sky} = T_{amb} - 6 \tag{9}$$

The heat transferred by convection are:

$$q_{c(w\_g)} = h_h(T_w - T_g) \tag{10}$$

$$q_{c(g\_a)} = h_a(T_g - T_{amb}) \tag{11}$$

Fig. 5. Typical weather condition and results of different heights of vapor chamber (H). (a) Solar irradiation on 2020, August 2nd. (b) Wind velocity and ambient temperature. (c) Water temperature at the evaporation surface (T_w) and the temperature of glass cover (T_g) of FSS for heights of vapor chamber H=2.5 cm and H=9.5 cm. (d) Experimental and theoretical productivity of FSS.

where h_h is the convective heat transfer coefficient in solar still, h_a is the convective heat transfer coefficient between the glass cover and the ambient.

The heat transferred from wick material to the basin is:

$$q_{d(w\_b)} = \frac{\lambda_i (T_w - T_{w,b})}{\delta_i} \qquad (12)$$

where λ_i is the thermal conductivity of the foam under the wick material, which is around 0.035 W/(m•K). $\delta_i = 0.02\ m$ is the thickness of the foam. $T_{w,b}$ is the temperature of the bulk water under the foam.

The heat transferred by phase change of vapor is:

$$q_{e(w\_g)} = h_{LV}\dot{m} \qquad (13)$$

where $\dot{m}$ is the productivity of the solar still, h_{LV} is obtained as [58]:

$$h_{LV} = h_{fg} + Cp_v(T_w - T_g) \qquad (14)$$

$$h_{fg} = 1.91846 \times 10^6 \left[\frac{T_s}{T_s - 33.91} \right]^2 \qquad (15)$$

where h_{fg} is the latent heat of vapor. Cp_v is the specific heat capacity of the vapor, which is around 1900 J/(kg·K) at 20 -70°C.

$\dot{m}$ is decided by the condition of both evaporation and condensation surface, as well as the structure of the phase change chamber. $\dot{m}$ can be obtained by [59]:

$$\dot{m} = h_m(\rho_{v,w} - \rho_{v,g}) \qquad (16)$$

where h_m is the convective mass transfer coefficient between evaporation surface and glass cover, $\rho_{v,w}$ and $\rho_{v,g}$ are the density of water vapor in the saturated air at the evaporation surface and the glass cover, respectively.

The density is related to the saturated vapor pressure, P_s, and the temperature of the saturated vapor T_s:

$$\rho_v = \frac{P_s}{R_{g,v}T_s} \qquad (17)$$

where $R_{g,v} = 461\ J/(kg \cdot K)$ is the gas constant of vapor, the saturated vapor pressure is determined by T_s [9]:

$$P_s = e^{\left(25.317 - \frac{5144}{T_s}\right)} \qquad (18)$$

The total pressure P in the vapor chamber is regarded as the ambient air pressure 101325 kPa, due to the chamber is connected to the ambient through water feeding and rejecting pipes.

The convective mass transfer coefficient h_m can be obtained by using the heat and mass transfer analogy. For heat transfer in a small horizontal chamber with the hot surface at the bottom, the Nusselt number is described as [60]:

$$Nu = 0.212(GrPr)^{\frac{1}{4}} \qquad (19)$$

$$h_h = \frac{Nu\lambda_a}{H} \qquad (20)$$

where Gr and Pr are the Grashof number and Prandtl number, respectively. λ_a is the thermal conductivity of the air. Gr and Pr are
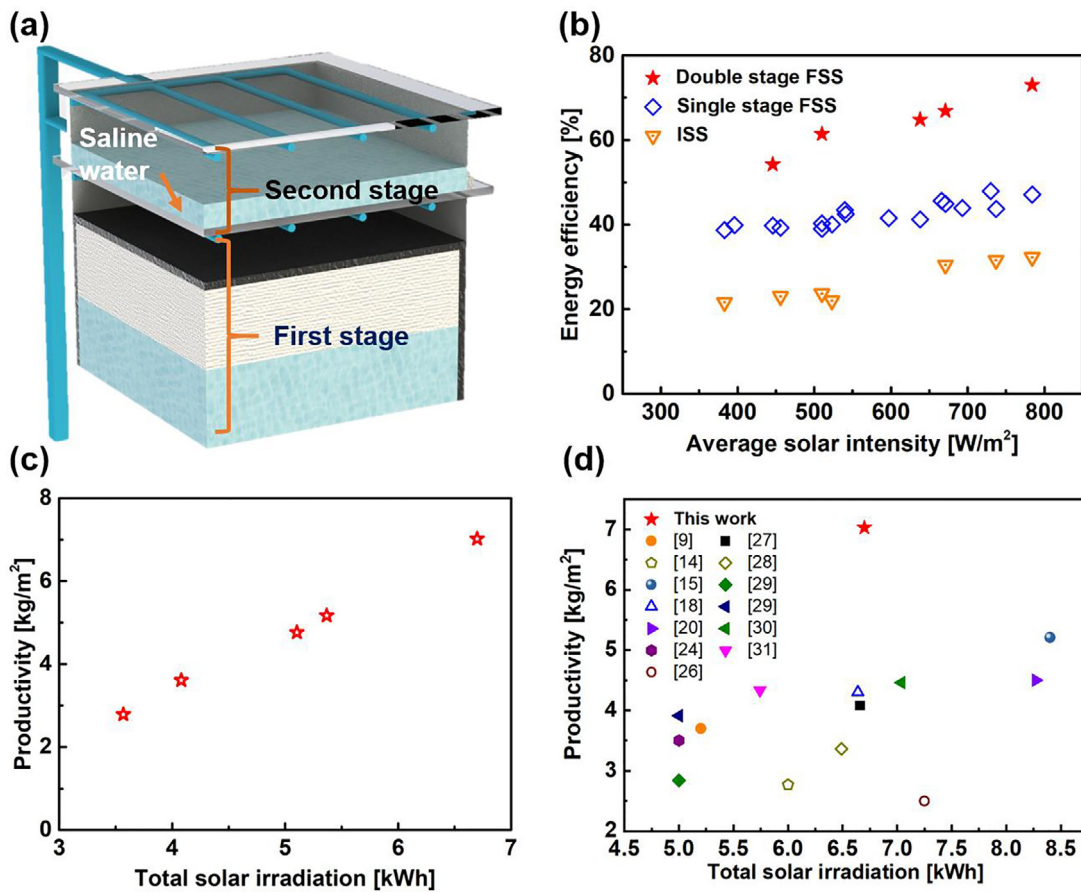
Fig. 6. Performance of the double-stage FSS. (a) The schematic diagram of double-stage FSS. (b) The energy efficiency of double stage FSS, single-stage FSS, and ISS under different average solar intensities. (c) Accumulated daily productivity of the double-stage FSS under different daily solar irradiation. (d) Daily productivity of solar still in this work (2 stages) and in references (continuously working at least 8 hours, one or two stages).

defined as:

$$Gr = \frac{g\alpha_v \Delta T H^3}{\nu^2} \tag{21}$$

$$Pr = \frac{\nu}{\alpha} \tag{22}$$

where g is the gravitational acceleration, $\alpha_v = 1/T_s$ is the volume expansion coefficient of moist air and α is the thermal diffusivity of moist air, H is the height of the vapor chamber in FSS. ΔT is the temperature difference between the evaporation surface and the glass cover, ν is the kinematic viscosity of moist air.

Based on the heat and mass transfer analogy, we have [59]:

$$\frac{h_h}{h_m} = \rho_a C p_a Le^{2/3} \tag{23}$$

where Le is the Lewis number:

$$Le = \frac{\alpha}{D} \tag{24}$$

where D is the diffusion coefficient of water vapor in the air:

$$D = D_{298K}\left(\frac{T_s}{298}\right)^{1.5} \tag{25}$$

where $D_{298K} = 0.256 \times 10^{-4} \mathrm{m^2/s}$ is the diffusion coefficient at 298K.

The thermophysical property of the saturated moist air can be obtained by the following equations [61]:

$$\alpha_a = SA_0 + SA_1 t + SA_2 t^2 + SA_2 t^3 + SA_4 t^4 \tag{26}$$

Table 3
List of coefficients for calculating the thermophysical property of the saturated moist air (0 – 100 °C) [61].

	0	1	2	3	4
SA	1.847E-5	1.162E-7	2.373E-10	-5.769E-12	-6.369E-14
SV	1.716E-5	4.722E-8	-3.663E-10	1.873E-12	-8.050E-14
SK	24.007E-3	7.278 E-5	-1.788E-7	-1.352E-9	-3.322E-11
SD	1.293	-5.538E-3	3.860E-5	-5.254E-7	–

$$\nu_a = SV_0 + SV_1 t + SV_2 t^2 + SV_2 t^3 + SV_4 t^4 \tag{27}$$

$$\lambda_a = SK_0 + SK_1 t + SK_2 t^2 + SK_2 t^3 + SK_4 t^4 \tag{28}$$

$$\rho_a = SD_0 + SD_1 t + SD_2 t^2 + SD_2 t^3 \tag{29}$$

The value of coefficients in the equations are listed in Table 3, t is the average temperature of the moist air in degree Celsius. Based on the above equations and the temperatures measured by the experiments, the theoretical productivity of FSS can be obtained.

3. Results and discussions

Firstly, mini-prototypes of both FSS and ISS were made and investigated indoor by using a solar simulator. The inner volume of the small FSS is 5 cm (length) × 5 cm (width) × 3 cm (height). The intensity of solar irradiation from the solar simulator is fixed at 1kW/m² unless otherwise mentioned. The FSS with UG and SG

Table 4
Comparison of flat solar still with other solar stills in references.

Ref.	Productivity kg/(m²•day)	Daily solar irradiation kWh/m²	Efficiency %	Working time	Stage number	Type of solar still
This work	7.03	6.7	72	9:00-17:00	2	Flat solar still
This work	4.5	6.7	46	9:00-17:00	1	Flat solar still
[9]	3.7	5.2	41.8	9:00-17:00	1	Single slope solar still
[14]	2.77	6	28.2	8:00-18:00	1	Stepped solar still
[15]	5.21	8.4	40.9	8:00-18:00	1	Stepped solar still integrates basin still
[18]	4.3	6.64	39	9:00-17:00	1	Wick type solar still
[20]	4.5	8.27	-	7:00-18:00	1	Wick type double slope solar still
[24]	3.5	5	-	9:00-20:00	1	Single slope solar still
[26]	2.5	7.25	-	7:00-18:00	1	Single slope solar still
[27]	4.08	6.66	40.8	7:00-19:00	1	Single slope solar still
[28]	3.36	6.49	37.1	8:00-21:00	1	Single slope solar still
[29]	2.84	5	32	8:00-16:00	1	Single slope solar still
[29]	3.91	5	44	8:00-16:00	2	Single slope solar still
[30]	4.46	7.04	39.3	8:00-18:00	1	Single slope solar still
[31]	4.33	5.74	41	7:00-18:00	1	Wick type solar still

were compared by the small-scale system. The hourly water productivity of the small FSS with UG is 0.75 kg/(m²•h) which is 70% higher than that of using SG (Fig. 3a). This indicates that the ultra-hydrophilic treatment of glass is very important for improving the system performance of FSS. The productivity of a small conventional ISS was also measured. It shows that there is barely freshwater collected after two hours (Fig. 3a).

Besides the effect of the glass cover, the effect of cotton threads is also studied from the aspect of the number of threads (Fig. 3b) and the length of vertical threads (Fig. 3c). The number of the thread refers to how many threads are attached to the glass cover parallelly and uniformly. The energy efficiency increases very slightly when the number of threads increases (Fig. 3b). The difference between 0.4 cm^{-1} and 1.2 cm^{-1} is less than 8%. Energy efficiency nearly converged to 54% after 0.8 cm^{-1}. It can be concluded that the cotton threads have very excellent water collection ability because the system performance is not greatly affected when only a few threads are used. This conclusion can be further proved by the effect of the length of vertical threads, L_t. The water collection is not affected even when L_t is only 2 cm, which means that even a very short vertical thread can provide enough driving force for water collection (Fig. 3c).

The temperatures of FSS in laboratory conditions are also measured (Fig. 3d). The temperature of both glass cover (T_g) and water at the evaporation surface (T_g) raise very quickly during the first several minutes, which indicates a great solar absorption and phase change performance in FSS. After 30 minutes, the temperature is nearly converged and raises very slowly. The temperature of water at the evaporation surface and glass cover reach up to 70°C and 65°C, respectively, after two hours of the experiment.

Based on the results of laboratory experiments, outdoor experiments were also carried out by homemade prototypes of FSS and ISS. 23 days of outdoor experiments were carried out and compared, including heavily cloudy days, cloudy days, and sunny days. Fig. 4a and b show the photos of outdoor experiments and the top view of FSS. The basin area for both ISS and FSS is 25 cm × 25 cm. Water with 3.5 wt% NaCl was premixed and placed in the basin. Bottles are used to contain the collected fresh water and the rejected brine. Fig. 4c shows the schematic diagram of the measurement setup in outdoor experiments. The solar intensity was measured and recorded every 5 seconds. The temperature of ambient and devices is measured by thermal couples and thermometer every hour. The mass of collected freshwater was measured every hour by the electronic balance. The solar stills and all components of the system were manufactured and tested in Shaoyang, Hunan, China (Latitude 26.99° N and longitude 111.27°E), from June to August 2020. The daily ambient temperature is around 30°C, the solar irradiation various a lot due to the different weather condition.

For more information about the temperature and solar irradiation of outdoor experiments, please refer to Supplementary Information VII.

The daily productivity of FSS and ISS under different solar irradiation is shown in Fig. 4d. The productivity of both FSS and ISS increases nearly linearly with the increase of daily solar irradiation. Around 4.3 kg/m² and 3 kg/m² of freshwater can be obtained under 6.3 kWh/m² of daily irradiation for FSS and ISS, respectively. It worth to be noted that the cotton threads in the FSS block near 10% of the solar irradiation. Therefore, it can be expected that the productivity of FSS can be further enhanced by replacing the cotton threads with other transparent materials. Besides, FSS shows great salt rejecting ability and there is no salt crystallization in FSS during the experimental days, which enables FSS to work continuously for a long time. Details of salt rejecting analysis can be found in Supplementary Information, Section V.

To investigate the importance of the compact structure of FSS, the performance of FSS is studied at two different heights of vapor chamber (H), namely the distance from the evaporation surface to the glass cover. H=2.5 is a typical compact structure of FSS. On the other hand, H=9.5 cm is much larger, which is similar to the average height of the vapor chamber in ISS. The results of a typical day (2020, August 2nd) are illustrated in Fig. 5. The total daily solar irradiation of this day is 5.7 kWh/m² (Fig. 5a). The ambient temperature is around 30°C and it is breezeless during the day (Fig. 5b).

Fig. 5c shows the temperature of glass and water of FSS under solar irradiation. The maximum temperature of water and glass cover in FSS with H=2.5 reach up to 66°C and 59°C, respectively. However, the maximum temperature of water and glass cover are only 62°C and 55°C, respectively, for H=9.5 cm. The temperature of H=2.5 cm is always higher than that of H=9.5 by 1-5 °C during the day, which shows the better thermal performance of the compact structure.

The hourly productivity of FSS is shown in Fig. 5d. It should be noted that the condensate water on the insulated four walls is also collected to exclude the effect of insufficient water collection. The results show that the accumulated productivity decreases around 38%, from 3.6 kg/m² to 2.6 kg/m², when H increase from 2.5 to 9.5 cm. To uncover the mechanism of the difference, the theoretical model of convective mass transfer is derived based on the analogy of heat and mass transfer as shown in section "theoretical model". The results reveal that the theoretical analysis agrees well with the experimental results, which indicates that the difference in productivity is mainly attributed to the different mass transfer rates in FSS. Therefore, the compact configuration of FSS is a very important advantage for improving the productivity of solar still due to the enhanced convective mass transfer.

Besides the improved mass transfer due to the compact structure, FSS can also be very easily extended to more stages for latent heat recovery. Fig. 6(a) shows the schematic diagram of a double-stage FSS. The majority of the solar irradiation passes the double layers of the glass cover and absorbed by the black wick materials of the first stage. The water evaporates after heated and condenses on the glass cover of the first stage. A few saline waters flow across the glass cover of the first stage to absorb the released latent heat and then evaporates. The vapor generated at the second stage condenses on the glass cover above it and is collected by cotton threads as in the first stage. The energy efficiency of double stage FSS under different solar intensities is shown in Fig. 6b. It is observed that the energy efficiency of the double stage FSS is sensitive to the solar intensity. When the mean solar intensity increase from 440 W/m^2 to 780 W/m^2, the energy efficiency of double stage FSS increase from 53% to 72%. This enhancement is higher than that of single-stage FSS and ISS, which indicates that the superiority of a double-stage FSS will be more obvious when higher solar intensity is available, such as using solar still with the solar concentrator.

The daily productivity of the double-stage FSS reaches up to 7.02 kg/m^2 under 6.7 kWh/m^2 of solar irradiation, i.e. 1.05 kg/kWh which is around 60% higher than that of single-stage FSS (Fig. 6c). Higher productivity can be expected when the solar irradiation is higher during a clear day. Meanwhile, 2.8 kg/m^2 of freshwater can be obtained even when the solar irradiation is very weak during an overcast day (3.6 kWh/m^2). The high productivity of double stage FSS shows the effectiveness and importance of latent heat recovery in solar still. Overall, the FSS proposed in this work shows great performance compared to other conventional solar stills in references. The productivity of conventional solar stills with various modification are usually between 3-5 kg/m^2 which is much lower than the double stage FSS as shown in Fig. 6d and Table 4. It should be noted that many further modifications can be applied to FSS, such as advanced materials for solar evaporation and condensation [40,62], solar collector or concentrator [63], glass cooling [64], reflectors [65], and so on. The prototype of FSS in this work is only an example and better performance can be expected with more modifications.

4. Conclusion

In conclusion, based on the ultra-hydrophilic glass, cotton threads, wick materials, and nanoparticles, a highly efficient and compact flat solar still is proposed. The indoor results show that the wettability of glass is a very important factor in FSS. The hourly productivity of FSS using ultra-hydrophilic glass is 70% higher than that of using ordinary glass. Meanwhile, the number of threads attached to the glass for freshwater collection also affects productivity. The productivity increases a little when the number of threads increases from 0.4 to 1.2 cm^{-1}. Moreover, the length of the thread at vertical direction doesn't affect the productivity for the range from 2 cm to 10 cm.

Furthermore, the performance of FSS is studied outdoor under natural solar irradiation. FSS could work continuously without salt crystallization on the evaporation surface. Experimental results show that the compact structure is very important for improving the productivity of FSS. Productivity decreases more than 30% when the height of the vapor chamber increases from 2.5 cm to 9.5 cm. Theoretical analysis reveals that the convective mass transfer in the vapor chamber can be enhanced by the compact structure hence higher productivity. The daily productivity of single-stage FSS reaches 4.3 kg/m^2 under 6.3 kWh/m^2 of solar irradiation. Furthermore, due to the latent heat recovery, the daily productivity of double-stage FSS reaches up to 7.02 kg/m^2 under 6.7 kWh/m^2 of solar irradiation, which is significantly higher than the conven-

tional solar still. The high performance of FSS shows its great potential for practical application.

Declaration of Competing Interest

There are no conflicts of interest to declare.

CRediT authorship contribution statement

Guilong Peng: Conceptualization, Methodology, Formal analysis, Writing – original draft, Investigation, Funding acquisition. **Swellam W. Sharshir:** Methodology, Formal analysis, Writing – original draft, Investigation. **Zhixiang Hu:** Resources, Formal analysis. **Rencai Ji:** Investigation, Formal analysis. **Jianqiang Ma:** Investigation. **A.E. Kabeel:** Writing – review & editing. **Huan Liu:** Resources. **Jianfeng Zang:** Resources. **Nuo Yang:** Conceptualization, Supervision, Writing – original draft, Funding acquisition.

Supplementary materials

Supplementary material associated with this article can be found, in the online version, at doi:10.1016/j.ijheatmasstransfer.2021.121657.

References

[1] M.A. Shannon, P.W. Bohn, M. Elimelech, J.G. Georgiadis, B.J. Marinas, A.M. Mayes, Science and technology for water purification in the coming decades, Nature 452 (7185) (2008) 301–310.

[2] M. Elimelech, W.A. Phillip, The future of seawater desalination: energy, technology, and the environment, Science 333 (6043) (2011) 712–717.

[3] L. Zhou, Y. Tan, J. Wang, W. Xu, Y. Yuan, W. Cai, S. Zhu, J. Zhu, 3D self-assembly of aluminium nanoparticles for plasmon-enhanced solar desalination, Nat. Photonics 10 (6) (2016) 393–398.

[4] P. Tao, G. Ni, C. Song, W. Shang, J. Wu, J. Zhu, G. Chen, T. Deng, Solar-driven interfacial evaporation, Nat. Energy 3 (12) (2018) 1031–1041.

[5] A.E. Kabeel, M. Abdelgaied, M.B. Feddaoui, Hybrid system of an indirect evaporative air cooler and HDH desalination system assisted by solar energy for remote areas, Desalination 439 (2018) 162–167.

[6] S.W. Sharshir, N. Yang, G. Peng, A.E. Kabeel, Factors affecting solar stills productivity and improvement techniques: a detailed review, Appl. Therm. Eng. 100 (2016) 267–284.

[7] P. Durkaieswaran, K.K. Murugavel, Various special designs of single basin passive solar still – a review, Renew. Sustain. Energy Rev. 49 (2015) 1048–1060.

[8] A.K. Kaviti, A. Yadav, A. Shukla, Inclined solar still designs: aa review, Renew. Sustain. Energy Rev. 54 (2016) 429–451.

[9] S.W. Sharshir, G. Peng, A.H. Elsheikh, E.M.A. Edreis, M.A. Eltawil, T. Abdelhamid, A.E. Kabeel, J. Zang, N. Yang, Energy and exergy analysis of solar stills with micro/nano particles: a comparative study, Energy Convers. Manage. 177 (2018) 363–375.

[10] P. Vishwanath Kumar, A. Kumar, O. Prakash, A.K. Kaviti, Solar stills system design: a review, Renew. Sustain. Energy Rev. 51 (2015) 153–181.

[11] Y. Yang, R. Zhao, T. Zhang, K. Zhao, P. Xiao, Y. Ma, P.M. Ajayan, G. Shi, Y. Chen, Graphene-based standalone solar energy converter for water desalination and purification, ACS Nano 12 (1) (2018) 829–835.

[12] H. Geng, Q. Xu, M. Wu, H. Ma, P. Zhang, T. Gao, L. Qu, T. Ma, C. Li, Plant leaves inspired sunlight-driven purifier for high-efficiency clean water production, Nat. Commun. 10 (1) (2019) 1512.

[13] A.E. Kabeel, Z.M. Omara, M.M. Younes, Techniques used to improve the performance of the stepped solar still—a review, Renew. Sustain. Energy Rev. 46 (2015) 178–188.

[14] A. Shyora, K. Patel, H. Panchal, Comparative analysis of stepped and single basin solar still in climate conditions of Gandhinagar Gujarat during winter, Int. J. Ambient Energy (2019) 1–11.

[15] R. Samuel Hansen, K. Kalidasa Murugavel, Enhancement of integrated solar still using different new absorber configurations: an experimental approach, Desalination 422 (2017) 59–67.

[16] W.M. Alaian, E.A. Elnegiry, A.M. Hamed, Experimental investigation on the performance of solar still augmented with pin-finned wick, Desalination 379 (2016) 10–15.

[17] V. Manikandan, K. Shanmugasundaram, S. Shanmugan, B. Janarthanan, J. Chandrasekaran, Wick type solar stills: a review, Renew. Sustain. Energy Rev. 20 (2013) 322–335.

[18] A.M. Manokar, D.P. Winston, J.D. Mondol, R. Sathyamurthy, A.E. Kabeel, H. Panchal, Comparative study of an inclined solar panel basin solar still in passive and active mode, Sol. Energy 169 (2018) 206–216.

[19] L. Sahota, G.N.T. Shyam, Energy matrices, enviroeconomic and exergoeconomic analysis of passive double slope solar still with water based nanofluids, Desalination 409 (2017) 66–79.

[20] P. Pal, P. Yadav, R. Dev, D. Singh, Performance analysis of modified basin type double slope multi–wick solar still, Desalination 422 (2017) 68–82.

[21] W.H. Alawee, S.A. Mohammed, H.A. Dhahad, A.S. Abdullah, Z.M. Omara, F.A. Essa, Improving the performance of pyramid solar still using rotating four cylinders and three electric heaters, Process Saf. Environ. Protection 148 (2021) 950–958.

[22] S. Rashidi, N. Rahbar, M.S. Valipour, J.A. Esfahani, Enhancement of solar still by reticular porous media: experimental investigation with exergy and economic analysis, Appl. Therm. Eng. 130 (2018) 1341–1348.

[23] T. Arunkumar, A.E. Kabeel, K. Raj, D. Denkenberger, R. Sathyamurthy, P. Ragupathy, R. Velraj, Productivity enhancement of solar still by using porous absorber with bubble-wrap insulation, J. Clean. Prod. 195 (2018) 1149–1161.

[24] S.W. Sharshir, G. Peng, L. Wu, F.A. Essa, A.E. Kabeel, N. Yang, The effects of flake graphite nanoparticles, phase change material, and film cooling on the solar still performance, Appl. Energy 191 (2017) 358–366.

[25] M.M. Naim, M.A. Abd El Kawi, Non-conventional solar stills Part 1. Non-conventional solar stills with charcoal particles as absorber medium, Desalination 153 (1) (2003) 55–64.

[26] H.S. Deshmukh, S.B. Thombre, Solar distillation with single basin solar still using sensible heat storage materials, Desalination 410 (2017) 91–98.

[27] M.S. Yousef, H. Hassan, An experimental work on the performance of single slope solar still incorporated with latent heat storage system in hot climate conditions, J. Clean. Prod. 209 (2019) 1396–1410.

[28] S.M. Shalaby, E. El-Bialy, A.A. El-Sebaii, An experimental investigation of a v–corrugated absorber single-basin solar still using PCM, Desalination 398 (2016) 247–255.

[29] A.A. Al-Karaghouli, W.E. Alnaser, Performances of single and double basin solar-stills, Appl. Energy 78 (3) (2004) 347–354.

[30] A.K. Thakur, R. Sathyamurthy, S.W. Sharshir, A.E. Kabeel, M.R. Elkadeem, Z. Ma, A.M. Manokar, M. Arıcı, A.K. Pandey, R. Saidur, Performance analysis of a modified solar still using reduced graphene oxide coated absorber plate with activated carbon pellet, Sustain. Energy Technol. Assess. 45 (2021) 101046.

[31] H. Sharon, K.S. Reddy, D. Krithika, L. Philip, Experimental performance investigation of tilted solar still with basin and wick for distillate quality and enviro-economic aspects, Desalination 410 (2017) 30–54.

[32] S. Chen, P. Zhao, G. Xie, Y. Wei, Y. Lyu, Y. Zhang, T. Yan, T. Zhang, A floating solar still inspired by continuous root water intake, Desalination 512 (2021) 115133.

[33] Y. Shi, R. Li, Y. Jin, S. Zhuo, L. Shi, J. Chang, S. Hong, K.-C. Ng, P. Wang, A 3D photothermal structure toward improved energy efficiency in solar steam generation, Joule 2 (6) (2018) 1171–1186.

[34] H. Liu, Z. Huang, K. Liu, X. Hu, J. Zhou, Interfacial solar-to-heat conversion for desalination, Adv. Energy Mater. 9 (21) (2019) 1900310.

[35] M. Gao, P.K.N. Connor, G.W. Ho, Plasmonic photothermic directed broadband sunlight harnessing for seawater catalysis and desalination, Energy Environ. Sci. 9 (10) (2016) 3151–3160.

[36] V.-D. Dao, H.-S. Choi, Carbon-based sunlight absorbers in solar-driven steam generation devices, Global Chall. 2 (2) (2018) 1700094.

[37] X. Yin, Y. Zhang, Q. Guo, X. Cai, J. Xiao, Z. Ding, J. Yang, Macroporous double-network hydrogel for high-efficiency solar steam generation under 1 sun illumination, ACS Appl. Mater. Interfaces 10 (13) (2018) 10998–11007.

[38] Y. Wang, L. Zhang, P. Wang, Self-floating carbon nanotube membrane on macroporous silica substrate for highly efficient solar-driven interfacial water evaporation, ACS Sustain. Chem. Eng. 4 (3) (2016) 1223–1230.

[39] Z. Wang, T. Horseman, A.P. Straub, N.Y. Yip, D. Li, M. Elimelech, S. Lin, Pathways and challenges for efficient solar-thermal desalination, Sci. Adv. 5 (7) (2019) eaax0763.

[40] C. Chen, Y. Kuang, L. Hu, Challenges and opportunities for solar evaporation, Joule 3 (3) (2019) 683–718.

[41] Z. Liu, H. Song, D. Ji, C. Li, A. Cheney, Y. Liu, N. Zhang, X. Zeng, B. Chen, J. Gao, Y. Li, X. Liu, D. Aga, S. Jiang, Z. Yu, Q. Gan, Extremely cost-effective and efficient solar vapor generation under nonconcentrated illumination using thermally isolated black paper, Global Chall. 1 (2) (2017) 1600003.

[42] G. Ni, S.H. Zandavi, S.M. Javid, S.V. Boriskina, T.A. Cooper, G. Chen, A salt-rejecting floating solar still for low-cost desalination, Energy Environ. Sci. 11 (6) (2018) 1510–1519.

[43] L. Yi, S. Ci, S. Luo, P. Shao, Y. Hou, Z. Wen, Scalable and low-cost synthesis of black amorphous Al-Ti-O nanostructure for high-efficient photothermal desalination, Nano Energy 41 (2017) 600–608.

[44] L. Zhang, B. Tang, J. Wu, R. Li, P. Wang, Hydrophobic light-to-heat conversion membranes with self-healing ability for interfacial solar heating, Adv. Mater. 27 (33) (2015) 4889–4894.

[45] G. Xue, Q. Chen, S. Lin, J. Duan, P. Yang, K. Liu, J. Li, J. Zhou, Highly efficient water harvesting with optimized solar thermal membrane distillation device, Global Chall. 2 (5-6) (2018) 1800001.

[46] L. Huang, H. Jiang, Y. Wang, Z. Ouyang, W. Wang, B. Yang, H. Liu, X. Hu, Enhanced water yield of solar desalination by thermal concentrated multistage distiller, Desalination 477 (2020) 114260.

[47] Z. Xu, L. Zhang, L. Zhao, B. Li, B. Bhatia, C. Wang, K.L. Wilke, Y. Song, O. Labban, J.H. Lienhard, R. Wang, E.N. Wang, Ultrahigh-efficiency desalination via a thermally-localized multistage solar still, Energy Environ. Sci. 13 (2020) 830–839.

[48] E. Chiavazzo, M. Morciano, F. Viglino, M. Fasano, P. Asinari, Passive solar high-yield seawater desalination by modular and low-cost distillation, Nat. Sustainability 1 (12) (2018) 763–772.

[49] T. Rajaseenivasan, K.K. Murugavel, T. Elango, R.S. Hansen, A review of different methods to enhance the productivity of the multi-effect solar still, Renew. Sustain. Energy Rev. 17 (2013) 248–259.

[50] J. Xiong, G. Xie, H. Zheng, Experimental and numerical study on a new multi–effect solar still with enhanced condensation surface, Energy Convers. Manage. 73 (2013) 176–185.

[51] S.-F. Li, Z.-H. Liu, Z.-X. Shao, H.-S. Xiao, N. Xia, Performance study on a passive solar seawater desalination system using multi-effect heat recovery, Appl. Energy 213 (2018) 343–352.

[52] H. Ghasemi, G. Ni, A.M. Marconnet, J. Loomis, S. Yerci, N. Miljkovic, G. Chen, Solar steam generation by heat localization, Nat. Commun. 5 (2014) 4449.

[53] G. Peng, S.W. Sharshir, Y. Hu, R. Li, H. Liu, D. Ma, L. Wu, J. Zang, H. Liu, W. Yu, H. Xie, N. Yang, Low-cost high-efficiency solar steam generator by combining thin film evaporation and heat localization: Both experimental and theoretical study, Appl. Therm. Eng. 143 (2018) 1079–1084.

[54] Y. Chen, Y. Zhang, L. Shi, J. Li, Y. Xin, T. Yang, Z. Guo, Transparent superhydrophobic/superhydrophilic coatings for self-cleaning and anti-fogging, Appl. Phys. Lett. 101 (3) (2012) 033701.

[55] Y. Xiong, M. Lai, J. Li, H. Yong, H. Qian, C. Xu, K. Zhong, S. Xiao, Facile synthesis of ultra-smooth and transparent TiO2 thin films with superhydrophilicity, Surf. Coat. Technol. 265 (2015) 78–82.

[56] W.S.Y. Wong, N. Nasiri, A.L. Rodriguez, D.R. Nisbet, A. Tricoli, Hierarchical amorphous nanofibers for transparent inherently super-hydrophilic coatings, J. Mater. Chem. A 2 (37) (2014) 15575–15581.

[57] C. Elango, N. Gunasekaran, K. Sampathkumar, Thermal models of solar still—a comprehensive review, Renew. Sustain. Energy Rev. 47 (2015) 856–911.

[58] G. Peng, S. Deng, S.W. Sharshir, D. Ma, A.E. Kabeel, N. Yang, High efficient solar evaporation by airing multifunctional textile, Int. J. Heat Mass Transf. 147 (2020) 118866.

[59] A. Sadeghpour, Z. Zeng, H. Ji, N. Dehdari Ebrahimi, A.L. Bertozzi, Y.S. Ju, Water vapor capturing using an array of traveling liquid beads for desalination and water treatment, Sci. Adv. 5 (4) (2019) eaav7662.

[60] T.L. Bergman, F.P. Incropera, D.P. DeWitt, A.S. Lavine, Fundamentals of Heat and Mass Transfer, 7 ed, John Wiley & Sons, 2011.

[61] P.T. Tsilingiris, Review and critical comparative evaluation of moist air thermophysical properties at the temperature range between 0 and 100°C for engineering calculations, Renew. Sustain. Energy Rev. 83 (2018) 50–63.

[62] J. Li, X. Wang, Z. Lin, N. Xu, X. Li, J. Liang, W. Zhao, R. Lin, B. Zhu, G. Liu, L. Zhou, S. Zhu, J. Zhu, Over 10 kg m−2 h−1 evaporation rate enabled by a 3D interconnected porous carbon foam, Joule 4 (2020) 1–10.

[63] R. Sathyamurthy, S.A. El-Agouz, P.K. Nagarajan, J. Subramani, T. Arunkumar, D. Mageshbabu, B. Madhu, R. Bharathwaaj, N. Prakash, A review of integrating solar collectors to solar still, Renew. Sustain. Energy Rev. 77 (2017) 1069–1097.

[64] S.W. Sharshir, G. Peng, L. Wu, N. Yang, F.A. Essa, A.H. Elsheikh, S.I.T. Mohamed, A.E. Kabeel, Enhancing the solar still performance using nanofluids and glass cover cooling: experimental study, Appl. Therm. Eng. 113 (2017) 684–693.

[65] Z.M. Omara, A.E. Kabeel, A.S. Abdullah, A review of solar still performance with reflectors, Renew. Sustain. Energy Rev. 68 (2017) 638–649.